Robust design against frequency variation for amplitude death in delay-coupled oscillators

Yoshiki Sugitani,[1,*] Kensei Kawahara,[2,†] and Keiji Konishi[1,‡]
[1]*Department of Electrical and Electronic Systems Engineering, Osaka Metropolitan University, 1-1 Gakuen, Naka-ku, Sakai, Osaka 599-8531, Japan*
[2]*Department of Electrical and Information Systems, Osaka Prefecture University, 1-1 Gakuen, Naka-ku, Sakai, Osaka 599-8531, Japan*

(Received 3 March 2024; accepted 23 May 2024; published 18 June 2024)

Amplitude death has the potential to suppress unwanted oscillations in various engineering applications. However, in some engineering applications, such as dc microgrids, airfoil systems, and thermoacoustic systems, oscillation frequency is highly susceptible to external influences, leading to considerable variations. To maintain amplitude death amidst these frequency variations, we propose a design procedure that is robust against frequency variation for inducing amplitude death in delay-coupled oscillators. We first analytically derive the oscillator frequency band in which amplitude death can occur. The frequency bandwidth is maximized when the coupling strength is inversely proportional to the connection delay. Furthermore, our analysis reveals that the oscillator frequency band is influenced by the minimum eigenvalue of the normalized adjacency matrix (i.e., network topology) and that bipartite networks exhibit limited robustness to frequency variations. Our design procedure maintains the stability of amplitude death even under substantial frequency variations and is applicable to various network topologies. Numerical simulations confirm the validity of the proposed design.

DOI: 10.1103/PhysRevE.109.064213

I. INTRODUCTION

Coupling interactions between oscillators can cause various interesting phenomena [1–9]. One notable phenomenon, amplitude death, leads to a uniform steady state, in which all the oscillators are quenched [10–16]. This phenomenon can be induced through various interactions, including static [17], dynamic [18], nonlinear [19], and conjugate connections [20].

Particular attention has been paid to delay connections, a natural consequence of signal propagation delays, which are ubiquitous in numerous systems [21]. Amplitude death resulting from such delay connections has been investigated theoretically [22] and experimentally [23–25]. Death by delay has potential in engineering applications, particularly in control engineering, because a reference signal is not required, the control signal is tiny after stabilization, and a signal propagation delay, which is inevitable, is used for stabilization [22].

Amplitude death can be used for suppressing unwanted oscillations in various engineering systems. In dc microgrids, for instance, the limit cycle of the bus voltage oscillation occurs due to a constant power load and causes voltage collapse [26,27]. By coupling microgrids, the limit cycle oscillation can be suppressed [28,29]. Similarly, in thermoacoustic systems, self-excited oscillation, which leads to the deterioration of gas turbine engines, emerges from the interplay of heat transfer and pressure variations [30,31]. Connecting thermoacoustic systems using tubes and valves can effectively suppress these oscillations [32–46]. For airfoil systems, flutter, a result of nonlinearities in plunge and pitch stiffness, can be quenched by connecting two airfoils with a spring [47–49].

To effectively achieve amplitude death in delay-coupled oscillators, it is crucial to correctly set the coupling parameters, namely, coupling strength and connection delay, in accordance with the oscillation frequency. Previous studies on amplitude death assumed a constant oscillation frequency. However, in practical engineering systems, the oscillation frequency is subject to variation due to external influences. For instance, in dc microgrids, load variations alter capacitance and inductance, impacting the frequency of bus voltage oscillations [50,51]. Similarly, the oscillatory behavior of thermoacoustic systems qualitatively changes in driving temperature [45,46]. For airfoil systems, the flutter frequency in airfoil systems varies with airspeed [52]. Therefore, despite successfully suppressing oscillations through delay coupling, there is a potential for the reoccurrence of the oscillation due to external factors causing frequency variations. To avoid the reoccurrence of the oscillation, a parameter design that can sustain the suppression of oscillation even amidst substantial frequency variations is required. However, to the best of our knowledge, the robustness of amplitude death against frequency variations has not been previously investigated.

To address this challenge, this paper proposes a design procedure for delay-coupled oscillators, which maintains amplitude death despite significant frequency variations. Initially, we analytically derive the relationship between the oscillator frequency and the coupling parameters for inducing amplitude death. Our findings indicate an optimal coupling strength that maximizes the frequency bandwidth where amplitude death is achievable. Furthermore, our analysis reveals that the frequency bandwidth is influenced by the minimum

*Contact author: sugitani@omu.ac.jp
†Contact author: sab01046@osakafu-u.net
‡Contact author: konishi-ees@omu.ac.jp

eigenvalue of the normalized adjacency matrix and that bipartite networks exhibit limited resilience to frequency variations. The proposed design procedure can maintain the stability of amplitude death amidst frequency variations and is applicable across various network topologies. The efficacy of our design is confirmed through numerical simulations.

The following notations are used in this paper. $\mathbb{N}$ is the set of positive integers, and $\mathbb{N}_0$ is the set of non-negative integers. The imaginary unit is defined as $i := \sqrt{-1}$.

II. PAIR OF OSCILLATORS

Self-excited unwanted oscillations in various engineering systems, such as dc microgrids [53], permanent-magnet synchronous motors [54], airfoil systems [48], and thermoacoustic systems [55], arise through Hopf bifurcation [56]. When a system undergoes Hopf bifurcation, an operating point of the system loses stability, leading to the emergence of self-excited oscillations. The Stuart-Landau oscillator is known as the normal form of Hopf bifurcation, since the dynamics of systems close to Hopf bifurcation can be transformed into the Stuart-Landau oscillator [56]. Thus, many studies on delayed feedback control and amplitude death use the Stuart-Landau oscillator [10,57].

The Stuart-Landau oscillator with the state variable $z(t) \in \mathbb{C}$ at time t is governed by the equation $\dot{z}(t) = \{1 + i\omega - |z(t)|^2\}z(t)$, where ω is the frequency of the oscillator. This oscillator has a stable limit cycle with frequency ω and an unstable equilibrium point $z^* = 0$.

This section considers a pair of delay-coupled Stuart-Landau oscillators,

$$\begin{aligned}\dot{z}_1(t) &= \{1 + i\omega - |z_1(t)|^2\}z_1(t) + k(z_2(t-\tau) - z_1(t)),\\ \dot{z}_2(t) &= \{1 + i\omega - |z_2(t)|^2\}z_2(t) + k(z_1(t-\tau) - z_2(t)),\end{aligned} \tag{1}$$

where $z_j(t) \in \mathbb{C}$ $(j = 1, 2)$ is the state variable for the jth oscillator.[1] The second term on the right-hand side denotes the coupling signal, where $k \geqslant 0$ is the coupling strength and $\tau \geqslant 0$ is the connection delay.[2]

The coupled oscillators in Eq. (1) have the following homogeneous steady state:

$$[z_1^*, z_2^*]^{\mathrm{T}} = [0, 0]. \tag{2}$$

For decoupled oscillators [i.e., Eq. (1) with $k = 0$], steady state (2) is unstable. This paper considers stabilization of steady state (2) by a delay connection, which corresponds to a suppression of the oscillation in Eq. (1). We investigate the local stability of steady state (2).

[1]Using the averaging method in Ref. [58], delay-coupled van der Pol oscillators, which have been employed to model coupled thermoacoustic oscillators [33,34,44], can be transformed into Eq. (1).

[2]Delayed connections can be classified into diffusive and direct couplings [59]. This paper considers the former, since diffusive couplings are typically used to describe interactions in practical systems, such as coupled thermoacoustic systems [33–40,44,48,49].

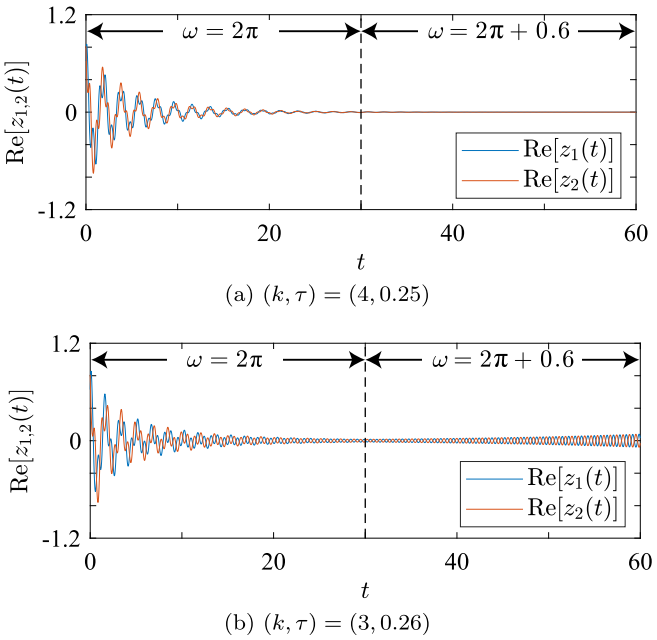

FIG. 1. Time-series data for Stuart-Landau oscillators described by Eq. (1). Here, the oscillators' frequency ω shifts from $\omega = 2\pi$ to $\omega = 2\pi + 0.6$ at $t = 30$. (a) demonstrates sustained amplitude death, while (b) shows the failure to maintain amplitude death after $t = 30$.

Linearizing Eq. (1) around steady state (2) yields the characteristic function $g_{\mathrm{AB}}(s)$ that governs the local stability of the steady state:

$$g_{\mathrm{AB}}(s) := g_{\mathrm{A}}(s)g_{\mathrm{B}}(s), \tag{3}$$

$$g_{\mathrm{A}}(s) := s - 1 - i\omega + k(1 - e^{-s\tau}), \tag{4}$$

$$g_{\mathrm{B}}(s) := s - 1 - i\omega + k(1 + e^{-s\tau}). \tag{5}$$

Steady state (2) is stable if and only if the dominant roots for both $g_{\mathrm{A}}(s) = 0$ and $g_{\mathrm{B}}(s) = 0$ lie within the open left-half of the complex plane.

A. Instability caused by frequency variation

This subsection presents a numerical example illustrating the loss of stability of steady state (2) due to variations in the frequency ω. Time-series data of the state variables in Eq. (1) are displayed in Figs. 1(a) and 1(b) for $(k, \tau) = (4, 0.25)$ and $(3, 0.26)$, respectively. The oscillator frequency ω is set to 2π for $t \in [0, 30)$, followed by a change to $2\pi + 0.6$ at $t = 30$. In both figures, up to $t = 30$, the state variables converge to steady state (2), indicating the occurrence of amplitude death. After $t = 30$, however, the variables in Fig. 1(b) begin oscillating, while stability is maintained in Fig. 1(a). This demonstrates that the stability of steady state (2) can be maintained even in the face of frequency variations if an appropriate set of coupling parameters (k, τ) is employed.

Figure 2 illustrates the stability regions in (k, τ) space where all the roots of Eq. (3) lie in the open left-half of the complex plane. The regions enclosed by the blue, black, and red curves, respectively, represent the stability regions for frequencies $\omega = 2\pi - 0.6$, 2π, and $2\pi + 0.6$. Amplitude death

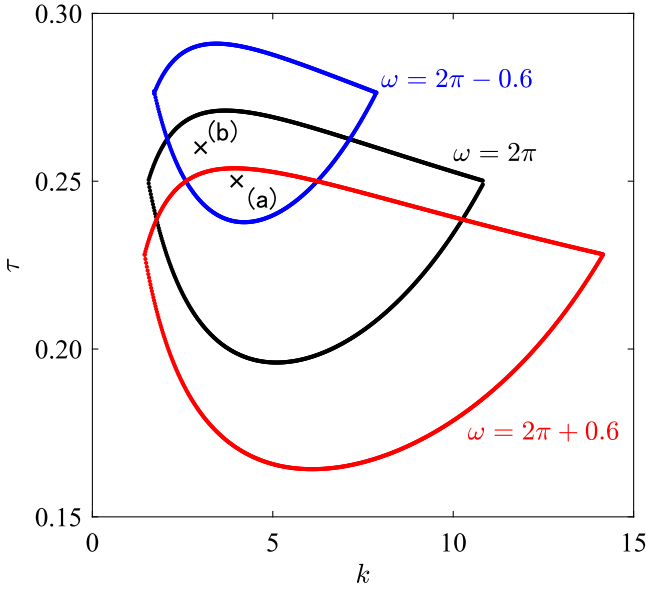

FIG. 2. Stability regions in (k, τ) space. The regions colored in blue, black, and red denote stability regions for $\omega = 2\pi - 0.6$, $\omega = 2\pi$, and $\omega = 2\pi + 0.6$, respectively. Points (a) and (b) correspond to the coupling parameter used in Figs. 1(a) and 1(b), respectively.

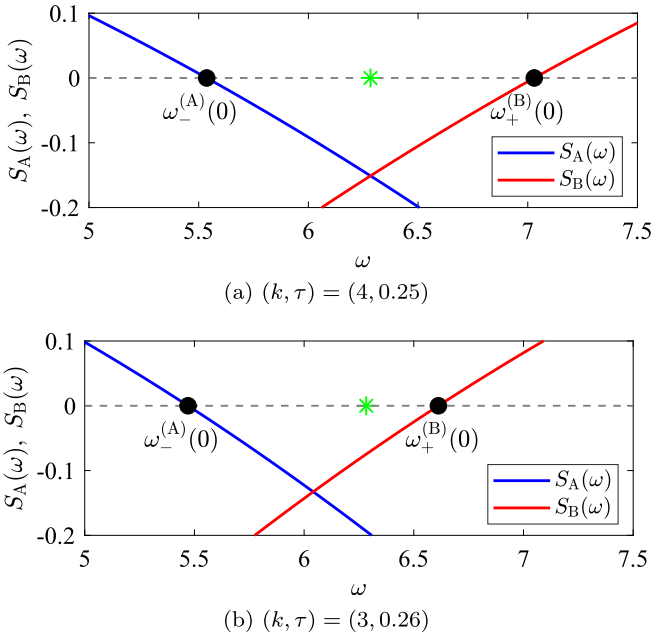

FIG. 3. Variation of the real part of dominant roots against frequency ω, for $g_A(s) = 0$ (blue) and $g_B(s) = 0$ (red). The coupling parameters in (a) and (b) correspond to points (a) and (b) in Fig. 2, respectively.

occurs for the parameter set (k, τ) in these regions. Points (a) and (b) in Fig. 2 correspond to the coupling parameters in Figs. 1(a) and 1(b), respectively. Point (a) is in the black and red regions; thus, the stability is maintained even after frequency shifts from $\omega = 2\pi$ to $\omega = 2\pi + 0.6$, as observed in Fig. 1(a). Conversely, Point (b) lies outside the red region, leading to a reemergence of oscillations after the frequency variation, as evident in Fig. 1(b). Notably, Point (a) is also in the blue region, suggesting a greater robustness against frequency variations compared to Point (b).

To ensure the persistence of amplitude death despite variations in frequency, it is critical to suitably design the coupling parameter set (k, τ). In this context, we consider a scenario where the oscillator frequency ω varies within the range $[\omega_n - \Delta\omega, \omega_n + \Delta\omega]$, with ω_n being the natural frequency of the oscillator, affected by external factors. Our objective is to devise a coupling parameter set (k, τ) capable of maintaining stability over the widest possible range of frequency variation $(\pm\Delta\omega)$. For instance, with a natural frequency of $\omega_n = 2\pi$, the coupling parameters at point (a) in Fig. 2 successfully sustain stability for a frequency change of $\pm\Delta\omega = \pm 0.6$.

Further examining the stability of steady state (2) relative to frequency ω, Fig. 3 illustrates the real part of the dominant roots for Eqs. (4) and (5), plotted against ω at points (a) and (b) in Fig. 2. The real parts of the dominant root for $g_A(s) = 0$ and $g_B(s) = 0$ are, respectively, expressed as

$$S_A(\omega) := \frac{1}{\tau}\mathrm{Re}[W_0(\tau k e^{-(1-k)\tau} e^{-i\omega\tau})] + 1 - k, \quad (6)$$

$$S_B(\omega) := \frac{1}{\tau}\mathrm{Re}[W_0(-\tau k e^{-(1-k)\tau} e^{-i\omega\tau})] + 1 - k, \quad (7)$$

where W_0 denotes the principal branch of the Lambert W function, satisfying $W(x)e^{W(x)} = x$ with $x \in \mathbb{C}$ [60,61]. The blue and red curves, $S_A(\omega)$ and $S_B(\omega)$, respectively, represent the real parts of dominant roots for $g_A(s) = 0$ and $g_B(s) = 0$. For stable $g_{AB}(s)$ [stable steady state (2)], both $S_A(\omega)$ and $S_B(\omega)$ must be negative. For example, at point (a) [see Fig. 3(a)], $g_{AB}(s)$ is stable from approximately $\omega = 5.536$ (which is less than $2\pi - 0.6$) to $\omega = 7.030$ (exceeding $2\pi + 0.6$), indicating a frequency bandwidth for stable $g_{AB}(s)$ of approximately 1.494. The principal aim of this paper is to maximize this frequency bandwidth, thereby enhancing the robustness of the coupling parameter set against frequency variations.

B. Frequency bandwidth for stable $g_{AB}(s)$

To identify the frequency band within which $g_A(s)$ and $g_B(s)$ remain stable, we analytically derive the frequencies at which stability changes, as indicated by the black dots in Fig. 3. When a root of $g_A(s) = 0$ is on the imaginary axis, $s = i\lambda$ $(\lambda \in \mathbb{R})$, the real and imaginary parts of $g_A(i\lambda) = 0$ are given by

$$-1 + k - k\cos\lambda\tau = 0, \quad (8)$$

$$\lambda - \omega + k\sin\lambda\tau = 0. \quad (9)$$

From Eqs. (8) and (9), we obtain λ that satisfies $g_A(i\lambda) = 0$:

$$\lambda_\pm := \omega \pm \sqrt{2k - 1}. \quad (10)$$

For coupling strength $k \geqslant 1/2$, a root s of $g_A(s) = 0$ intersects the imaginary axis at points $s = i\lambda_\pm$.

Consider the case with $\omega = 0$ and varying connection delay τ. At $\omega = 0$ and $\tau = 0$, we can see that $g_A(s) = 0$ has an unstable root $s = 1$. Since $\mathrm{sgn}(\mathrm{Re}[\frac{ds}{d\tau}]_{s=i\lambda_+}) > 0$ at $\omega = 0$, a root crosses the imaginary axis at $s = i\lambda_+$ from left to right

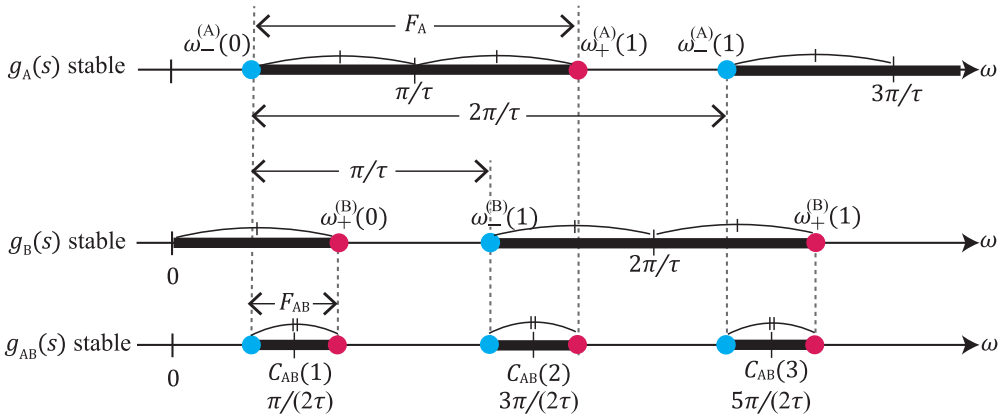

FIG. 4. Frequency band for stable $g_A(s)$, $g_B(s)$, and $g_{AB}(s)$ (i.e., Ω_A, Ω_B, and Ω_{AB}, respectively).

as τ increases from zero. We easily find that the crossing occurs at $\tau = \bar{\tau}(k) + \pi/\sqrt{2k-1}$, where

$$\bar{\tau}(k) := \frac{\pi - \phi(k)}{\sqrt{2k-1}}, \tag{11}$$

$$\phi(k) := \cos^{-1}\left(\frac{k-1}{k}\right) \in [0, \pi]. \tag{12}$$

Thus, $g_A(s) = 0$ with $\omega = 0$ has one unstable root for

$$k \geqslant \frac{1}{2}, \quad \tau \in \left[0, \bar{\tau}(k) + \frac{\pi}{\sqrt{2k-1}}\right). \tag{13}$$

Under Eq. (13), the crossing direction of the root $s = i\lambda_\pm$ with increasing ω can be calculated as

$$\mathrm{sgn}\left(\mathrm{Re}\left[\frac{ds}{d\omega}\right]_{s=i\lambda_\pm}\right) = \mathrm{sgn}(\lambda_\pm - \omega). \tag{14}$$

From Eqs. (10) and (14), the root crosses the imaginary axis from left to right at $s = i\lambda_+$ and from right to left at $s = i\lambda_-$ with an increase in ω. Furthermore, Eqs. (8)–(10) lead to

$$\sin\lambda_\pm\tau = \frac{\mp\sqrt{2k-1}}{k}, \tag{15}$$

$$\cos\lambda_\pm\tau = \frac{k-1}{k}. \tag{16}$$

From the sign of Eq. (15), we see that $\lambda_+\tau \in [\pi, 2\pi]$ and $\lambda_-\tau \in [0, \pi]$. Consequently, Eq. (16) informs us about the conditions that lead to the determination of crossing frequencies:

$$\begin{aligned} &\lambda_+\tau = 2l\pi - \phi(k), \quad l \in \mathbb{N}, \\ &\lambda_-\tau = 2l\pi + \phi(k), \quad l = 0, \pm1, \pm2, \ldots. \end{aligned} \tag{17}$$

Substituting Eq. (10) into Eqs. (17), we identify the specific frequencies at which roots cross the imaginary axis as

$$\begin{aligned} \omega_+^{(A)}(l) &:= \frac{2l\pi - \phi(k)}{\tau} - \sqrt{2k-1}, \quad l \in \mathbb{N}, \\ \omega_-^{(A)}(l) &:= \frac{2l\pi + \phi(k)}{\tau} + \sqrt{2k-1}, \quad l \in \mathbb{N}_0. \end{aligned} \tag{18}$$

As ω increases, the crossing at $\omega = \omega_+^{(A)}(l)$ for a rightward direction and at $\omega = \omega_-^{(A)}(l)$ for a leftward direction delineates the stabilizing $(\omega_-^{(A)}(l))$ and destabilizing $(\omega_+^{(A)}(l))$ frequencies. Notably, for stable $g_A(s)$, the first stabilizing frequency $\omega_-^{(A)}(0)$ must appear before the first destabilizing frequency $\omega_+^{(A)}(1)$ as ω increases from zero. The inequality $\omega_-^{(A)}(0) > \omega_+^{(A)}(1)$ can be rewritten as

$$\tau < \bar{\tau}(k). \tag{19}$$

Note that it is straightforward to confirm that $\omega_-^{(A)}(0) = \omega_+^{(A)}(1)$ when $k = 1/2$.

Summarizing the above, if k and τ satisfy

$$k > \frac{1}{2}, \quad \tau \in [0, \bar{\tau}(k)), \tag{20}$$

then $g_A(s) = 0$ has one unstable root for $\omega = 0$. With increasing ω from zero, $g_A(s)$ becomes stable at the first stabilizing frequency $\omega = \omega_-^{(A)}(0)$, as illustrated in the upper part of Fig. 4. Stability for $g_A(s)$ is then maintained up to the point where ω approaches the first destabilizing frequency $\omega_+^{(A)}(1)$. Therefore, $g_A(s)$ is stable between $\omega = \omega_-^{(A)}(0)$ and $\omega = \omega_+^{(A)}(1)$. Given the periodic occurrence of $\omega_+^{(A)}(l)$ and $\omega_-^{(A)}(l)$ in intervals of $2\pi/\tau$ with increasing l, the frequency band for stable $g_A(s)$ similarly demonstrates periodicity, as indicated by $S_A(\omega) = S_A(\omega + 2\pi/\tau)$. Moreover, due to the relationship between the real parts of the dominant roots for $g_A(s)$ and $g_B(s)$, where $S_A(\omega) = S_B(\omega - \pi/\tau)$, the frequency band for stable $g_B(s)$ is equivalent to that for stable $g_A(s)$ shifted by π/τ. The crossing frequencies for $g_B(s)$ can thus be expressed as follows:

$$\begin{aligned} \omega_+^{(B)}(l) &:= \frac{(2l+1)\pi - \phi(k)}{\tau} - \sqrt{2k-1}, \quad l \in \mathbb{N}_0, \\ \omega_-^{(B)}(l) &:= \frac{(2l-1)\pi + \phi(k)}{\tau} + \sqrt{2k-1}, \quad l \in \mathbb{N}, \end{aligned} \tag{21}$$

where $\omega_+^{(B)}(l)$ and $\omega_-^{(B)}(l)$ are the destabilizing and stabilizing frequencies, respectively (see the middle part of Fig. 4). The frequency bands for stable $g_A(s)$ and $g_B(s)$ can be summarized as follows.

Lemma 1. Assume that k and τ satisfy Eq. (20). Characteristic function $g_A(s)$ is stable if and only if ω belongs to

$$\Omega_A := \bigcup_{l\in\mathbb{N}} \left(\omega_-^{(A)}(l-1), \omega_+^{(A)}(l)\right). \tag{22}$$

Characteristic function $g_{\mathrm{B}}(s)$ is stable if and only if ω belongs to

$$\Omega_{\mathrm{B}} := \left[0, \omega_{+}^{(\mathrm{B})}(0)\right) \cup \bigcup_{l\in\mathbb{N}} \left(\omega_{-}^{(\mathrm{B})}(l), \omega_{+}{}^{(B)}(l)\right). \tag{23}$$

Proof. The proof is omitted. ∎

From Lemma 1, we confirm that the center of the frequency band for stable $g_{\mathrm{A}}(s)$ is given by

$$C_{\mathrm{A}}(l) := \frac{2l-1}{\tau}\pi, \quad l \in \mathbb{N}, \tag{24}$$

and that for stable $g_{\mathrm{B}}(s)$ is given by

$$C_{\mathrm{B}}(l) := \frac{2l}{\tau}\pi, \quad l \in \mathbb{N}, \tag{25}$$

except for the first frequency band $\omega \in \left[0, \omega_{+}^{(B)}(0)\right)$ (see Fig. 4). Note that these center frequencies depend only on the connection delay. Furthermore, the frequency bandwidth for stable $g_{\mathrm{A}}(s)$ and that for stable $g_{\mathrm{B}}(s)$ except for the first frequency band are the same and are expressed as

$$F_{\mathrm{A}}(k,\tau) := \frac{2\pi - 2\phi(k)}{\tau} - 2\sqrt{2k-1}. \tag{26}$$

$g_{\mathrm{AB}}(s)$ is stable if and only if ω belongs to both Ω_{A} and Ω_{B}. We see that $\Omega_{\mathrm{AB}} := \Omega_{\mathrm{A}} \cap \Omega_{\mathrm{B}}$ exists for $\omega_{+}^{(\mathrm{B})}(l) > \omega_{-}^{(\mathrm{A})}(l)$. This inequality is satisfied if and only if

$$k > 1, \quad \tau \in [0, \bar{\tau}_{\mathrm{AB}}(k)), \tag{27}$$

where

$$\bar{\tau}_{\mathrm{AB}}(k) := \frac{1}{2}\left(\bar{\tau}(k) - \frac{\phi(k)}{\sqrt{2k-1}}\right). \tag{28}$$

The following lemma summarizes the frequency band for stable $g_{\mathrm{AB}}(s)$.

Lemma 2. Under Eq. (27), $g_{\mathrm{AB}}(s) = g_{\mathrm{A}}(s)g_{\mathrm{B}}(s)$ is stable if and only if ω belongs to

$$\Omega_{\mathrm{AB}} := \bigcup_{l\in\mathbb{N}_0} \left(\omega_{-}^{(\mathrm{A})}(l), \omega_{+}^{(\mathrm{B})}(l)\right) \cup \left(\omega_{-}^{(\mathrm{B})}(l+1), \omega_{+}^{(\mathrm{A})}(l+1)\right). \tag{29}$$

Proof. This is obvious from the preceding analysis and the observed periodicity of the frequency band for stable $g_{\mathrm{A}}(s)$ and $g_{\mathrm{B}}(s)$. ∎

Figure 4 graphically shows the frequency bands for stable $g_{\mathrm{A}}(s)$, $g_{\mathrm{B}}(s)$, and $g_{\mathrm{AB}}(s)$. The bold lines denote the sets Ω_{A}, Ω_{B}, and Ω_{AB}. We can see that the frequency band for stable $g_{\mathrm{AB}}(s)$ appears periodically in terms of ω. Each frequency bandwidth for stable $g_{\mathrm{AB}}(s)$ is given by

$$F_{\mathrm{AB}}(k,\tau) := \frac{\pi - 2\phi(k)}{\tau} - 2\sqrt{2k-1}, \tag{30}$$

which depends on k and τ, but is independent of l (see Fig. 4).

The goal of this paper is to design (k,τ) that maximizes the bandwidth $F_{\mathrm{AB}}(k,\tau)$, thereby enhancing the robustness against frequency variations. The frequency bandwidth can be maximized with respect to the coupling strength k as follows.

Lemma 3. Under Eq. (27), the frequency bandwidth $F_{\mathrm{AB}}(k,\tau)$ is maximized with respect to k at $k = 1/\tau$.

Proof. This can be confirmed by differentiating Eq. (30) with respect to k. ∎

Note that in Ref. [62], for a single Stuart-Landau oscillator with delayed feedback control, it is shown that $k = 1/\tau$ is the optimal feedback parameter value (i.e., that for which the stability is strongest). However, the frequency bandwidth is not discussed in Ref. [62].

The center of each frequency band for stable $g_{\mathrm{AB}}(s)$ (see Fig. 4) is given by

$$C_{\mathrm{AB}}(l) = \frac{2l-1}{2\tau}\pi, \quad l \in \mathbb{N}, \tag{31}$$

which depends only on the connection delay τ. In other words, the center frequency can be adjusted by varying τ.

III. DESIGN PROCEDURE FOR PAIR OF OSCILLATORS

Based on the results in the previous section, we propose a design procedure for the coupling parameter set (k,τ) that is robust against frequency variation.

Here, we consider the situation where the natural frequency of the oscillator $\omega = \omega_n$ is given. The design focuses on aligning the center of the first frequency band, $C_{\mathrm{AB}}(1) = \pi/(2\tau)$, with the given natural frequency ω_n, and on maximizing the frequency bandwidth $F_{\mathrm{AB}}(k,\tau)$.

Since the center point given in Eq. (31) depends only on τ, the center of the first frequency band, $C_{\mathrm{AB}}(1)$, can be aligned with the natural frequency ω_n by setting

$$\tau = \tau^* := \frac{\pi}{2\omega_n}. \tag{32}$$

From Lemma 3, the bandwidth $F_{\mathrm{AB}}(k,\tau)$ is maximized with respect to k when

$$k = k^* := 1/\tau^* = \frac{2\omega_n}{\pi}. \tag{33}$$

The maximized frequency bandwidth is given by

$$\begin{aligned} F_{\mathrm{AB}}^* &:= F_{\mathrm{AB}}(k^*,\tau^*) \\ &= \frac{2\omega_n}{\pi}\left\{\pi - 2\phi\left(\frac{2\omega_n}{\pi}\right)\right\} - 2\sqrt{\frac{4\omega_n}{\pi} - 1}. \end{aligned} \tag{34}$$

Positioning ω_n precisely at the center of the frequency band for stable $g_{\mathrm{AB}}(s)$ ensures stability for frequencies within the range $\omega \in [\omega_n - F_{\mathrm{AB}}^*/2,\ \omega_n + F_{\mathrm{AB}}^*/2]$. Summarizing the above, a design for a pair of oscillators that is robust against frequency variation is achieved as follows.

Theorem 1. Assume that ω_n satisfies

$$\frac{\pi}{2\omega_n} < \frac{\pi - 2\phi(2\omega_n/\pi)}{2\sqrt{4\omega_n/\pi - 1}}. \tag{35}$$

For $(k,\tau) = (k^*,\tau^*)$, the local stability of steady state (2) is maintained even if the frequency changes by up to $\pm F_{\mathrm{AB}}^*/2$.

Proof. The designed parameters $(k,\tau) = (k^*,\tau^*)$ satisfy Eq. (27) if Eq. (35) holds. It is obvious that for $(k,\tau) = (k^*,\tau^*)$, ω_n aligns with the center of the first frequency band for stable $g_{\mathrm{AB}}(s)$ and the stability is maintained for $\omega \in \left[\omega_n - F_{\mathrm{AB}}^*/2,\quad \omega_n + F_{\mathrm{AB}}^*/2\right]$. ∎

Furthermore, the following provides a simpler condition than Eq. (35).

Corollary 1. If ω_n satisfies

$$\omega_n \geqslant 2\pi, \tag{36}$$

then Eq. (35) holds.

As a design example, the natural frequency $\omega_n = 2\pi$, which satisfies Eq. (36), is given. Then, the parameter set $(k, \tau) = (k^*, \tau^*) = (4, 0.25)$ is obtained. This parameter set is used in Fig. 2(a). We can confirm that the natural frequency $\omega_n = 2\pi$ is in the center of the frequency band [see the green star in Fig. 3(a)]. The allowable frequency variation for maintaining stability is calculated as $\pm F^*_{\mathrm{AB}}/2 \simeq \pm 0.747$, thereby ensuring the stability of steady state (2) against frequency shifts approximately $\pm 12\%$ relative to ω_n.

IV. OSCILLATOR NETWORKS

This section expands upon the preceding discussion, applying the findings to a coupled oscillator network. We provide a design procedure applicable to any network topology aimed at ensuring robustness against frequency variations.

A. Frequency band for coupled oscillators

The dynamics of N coupled oscillators is given by

$$\dot{z}_j(t) = \{1 + i\omega - |z_j(t)|^2\} z_j(t) + u_j(t), \tag{37}$$

$$u_j(t) = k \sum_{l=1}^{N} \frac{a_{jl}}{d_j} (z_l(t-\tau) - z_j(t)), \tag{38}$$

where $j = 1, \ldots, N$. Here, $a_{jl} \in \{0, 1\}$ is the (j, l)th element of the adjacency matrix $\boldsymbol{A}$. If oscillator j is connected to oscillator l, $a_{jl} = a_{lj} = 1$; otherwise, $a_{jl} = a_{lj} = 0$. Self-feedback is forbidden (i.e., $a_{jj} = 0$). The degree of oscillator j is defined as $d_j := \sum_{l=1}^{N} a_{jl}$. Equations (37) and (38) have the following homogeneous steady state:

$$[z_1^* \cdots z_N^*]^{\mathrm{T}} = [0 \cdots 0]^{\mathrm{T}}. \tag{39}$$

The local stability of steady state (39) is governed by the characteristic function,

$$G(s) := \prod_{j=1}^{N} g(s, \rho_j), \tag{40}$$

$$g(s, \rho) := s - 1 - i\omega + k(1 - \rho e^{-s\tau}), \tag{41}$$

with ρ_j $(j = 1, \ldots, N)$ is the eigenvalue of the normalized adjacency matrix $\boldsymbol{A}_{\mathrm{n}} := \boldsymbol{D}^{-1}\boldsymbol{A}$, where $\boldsymbol{D} := \mathrm{diag}(d_1, \ldots, d_N)$ is the diagonal degree matrix. It is known that the eigenvalue ρ_j satisfies $\rho_1 = 1 \geqslant \rho_2 \geqslant \cdots \geqslant \rho_N \geqslant -1$ for any network topology [63]. Note that $g_{\mathrm{A}}(s)$ and $g_{\mathrm{B}}(s)$ in Eq. (3) correspond to $g(s, 1)$ and $g(s, -1)$, respectively. The real part of the dominant root is given by

$$S(\omega, \rho) := \frac{1}{\tau} \mathrm{Re}[W_0(\rho\tau k e^{-(1-k)\tau} e^{-i\omega\tau})] + 1 - k. \tag{42}$$

Due to $S(\omega, 0) = 1 - k$, the characteristic function $g(s, \rho)$ with $\rho = 0$ is stable independent of ω if and only if $k > 1$. For nonzero ρ, we can analytically derive the frequency band for stable $g(s, \rho)$ using a calculation similar to that in the previous section.

Lemma 4. Assume that k and τ satisfy

$$k \in \left(\frac{1}{1 + |\rho|}, \frac{1}{1 - |\rho|} \right], \quad \tau \in \left[0, \frac{\pi - \Phi(\rho, k)}{\sqrt{D(\rho, k)}} \right). \tag{43}$$

Characteristic function $g(s, \rho)$ with $\rho \neq 0$ is stable if and only if ω belongs to $\Omega^{(+)}$ for $\rho > 0$ and $\Omega^{(-)}$ for $\rho < 0$, where

$$\Omega^{(+)} := \bigcup_{l \in \mathbb{N}} \left(\omega_-^{(+)}(l-1, \rho), \omega_+^{(+)}(l, \rho) \right), \tag{44}$$

$$\Omega^{(-)} := \left[0, \omega_+^{(-)}(0, \rho) \right) \cup \bigcup_{l \in \mathbb{N}} \left(\omega_-^{(-)}(l, \rho), \omega_+^{(-)}(l, \rho) \right), \tag{45}$$

with

$$\omega_+^{(+)}(l, \rho) := \frac{2l\pi - \Phi(\rho, k)}{\tau} - \sqrt{D(\rho, k)}, \tag{46}$$

$$\omega_-^{(+)}(l, \rho) := \frac{2l\pi + \Phi(\rho, k)}{\tau} + \sqrt{D(\rho, k)}, \tag{47}$$

$$\omega_+^{(-)}(l, \rho) := \frac{(2l+1)\pi - \Phi(\rho, k)}{\tau} - \sqrt{D(\rho, k)}, \tag{48}$$

$$\omega_-^{(-)}(l, \rho) := \frac{(2l-1)\pi + \Phi(\rho, k)}{\tau} + \sqrt{D(\rho, k)}, \tag{49}$$

$$D(\rho, k) := (\rho^2 - 1)k^2 + 2k - 1, \tag{50}$$

$$\Phi(\rho, k) := \cos^{-1}\left(\frac{k-1}{|\rho| k} \right). \tag{51}$$

Proof. The crossing frequency can be derived using the same procedure as that used for $g_{\mathrm{A}}(s)$ and $g_{\mathrm{B}}(s)$. The proof is omitted. ■

From Lemma 4, we can see that the center of the frequency band for stable $g(s, \rho)$, for positive and negative ρ, is determined by Eqs. (24) and (25), respectively, regardless of the value of ρ. For larger values of k, the stability of $g(s, \rho)$ is maintained for all non-negative frequencies ω as follows.

Corollary 2. If the condition

$$k > \frac{1}{1 - |\rho|}, \quad |\rho| \neq 1, \tag{52}$$

holds, then characteristic function $g(s, \rho)$ is stable for any $\omega \geqslant 0$.

Proof. $g(s, \rho)$ with $\omega = 0$ is stable if Eq. (52) is satisfied [64]. It is easily confirmed that the stability of $g(s, \rho)$ never changes as ω increases from 0. ■

Let Ω_{ρ_j} be the frequency set for stable $g(s, \rho_j)$. For steady state (39) to be stable, the frequency ω must belong to all the sets Ω_{ρ_j} $(j = 1, \ldots, N)$. This implies that there must be an intersection of all the frequency sets Ω_{ρ_j} $(j = 1, \ldots, N)$. By deriving the condition for the existence of such an intersection, the stability of $G(s)$ is summarized as follows.

Lemma 5. Assume that k and τ satisfy

$$k \in \left(1, \frac{1}{1 + \rho_N} \right], \quad \tau \in \left[0, \frac{\pi - \Phi(\rho_N, k) - \Phi(1, k)}{\sqrt{D(\rho_N, k)} + \sqrt{D(1, k)}} \right). \tag{53}$$

Characteristic function $G(s)$ is stable if and only if ω belongs to

$$\Omega := \bigcup_{l \in \mathbb{N}_0} \left(\left(\omega_-^{(+)}(l, 1), \omega_+^{(-)}(l, \rho_N) \right) \cap \left(\omega_-^{(-)}(l+1, \rho_N), \omega_+^{(+)}(l+1, 1) \right) \right). \tag{54}$$

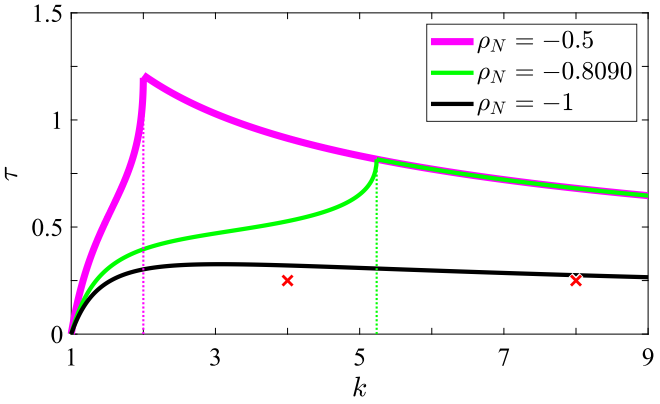

FIG. 5. Coupling parameter areas that satisfy Eqs. (53) and (55), in which the frequency band for stable $G(s)$ exists.

In addition, under the condition

$$k > \frac{1}{1+\rho_N}, \quad \tau \in [0, \bar{\tau}(k)), \quad \rho_N > -1, \tag{55}$$

$G(s)$ is stable if and only if ω belongs to $\Omega_{\rm A}$.

Proof. See Appendix. ■

We can see that Lemma 5 is the extended version of Lemma 2 since Ω in Eq. (54) is equivalent to $\Omega_{\rm AB}$ in Eq. (29) when $\rho_N = -1$. Lemma 5 shows that under Eq. (53), the frequency set for stable $G(s)$, which is the intersection of all Ω_{ρ_j} $(j = 1, \ldots, N)$, is given by the intersection of Ω_{ρ_1} and Ω_{ρ_N}. Roughly speaking, the smallest and largest eigenvalues (ρ_1 and ρ_N) fundamentally govern the determination of the frequency set for stable $G(s)$. In addition, under Eq. (55), the frequency set for stable $G(s)$ is the same as Ω_{ρ_1}.

Figure 5 shows the parameter areas that satisfy Eqs. (53) and (55) for $\rho_N = -0.5, -0.8090$, and -1. The pink and green dotted lines denote $k = 1/(1+\rho_N)$ for $\rho_N = -0.5$ and -0.8090, respectively. In the area to the left of the pink (green) dotted line and below the pink (green) solid curve, Eq. (53) with $\rho_N = -0.5$ ($\rho_N = -0.8090$) holds. The area to the right of the pink (green) dotted line and below the pink (green) solid curve satisfies Eq. (55) with $\rho_N = -0.5$ ($\rho_N = -0.8090$). The area below the black curve satisfies Eq. (53) with $\rho_N = -1$. In these areas, there exists a frequency ω for stable $G(s)$. We can see that the parameter space expanding as ρ_N increases.

Figures 6 and 7 show the real part of the dominant roots of $g(s, \rho) = 0$, denoted as $S(\omega, \rho)$, against ω for ring networks comprising $N = 12$ and $N = 5$ oscillators, respectively. The minimum eigenvalues ρ_N for these networks are $\rho_{12} = -1$ and $\rho_5 = \cos(4\pi/5) \simeq -0.8090$. The connection delay is fixed at $\tau = 0.25$. The coupling strength is set to $k = 4$ for Figs. 6(a) and 7(a) and $k = 8$ for Figs. 6(b) and 7(b). These coupling parameters satisfy Eqs. (53) or (55), as highlighted by the red cross marks in Fig. 5.

In Figs. 6 and 7, each curve corresponds to $S(\omega, \rho_j)$ for a specified ρ_j, using the notation $\rho_{j,l}$ to indicate $\rho_j = \rho_l$. Red and blue curves denote the dominant roots for the negative and positive eigenvalues, respectively, and bold curves represent $S(\omega, \rho_1)$ and $S(\omega, \rho_N)$. The crossing frequencies marked as

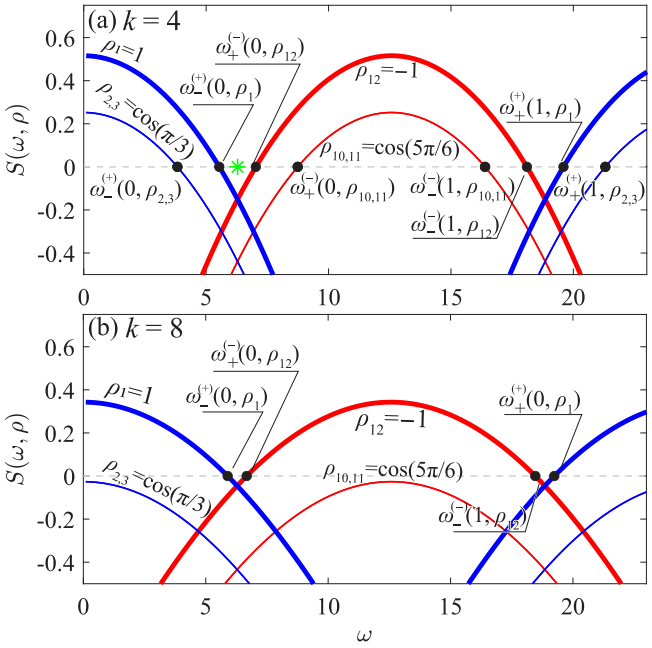

FIG. 6. Real part of dominant roots for $g(s, \rho_j) = 0$, $S(\omega, \rho)$, for ring network with $N = 12$ ($\tau = 0.25$): (a) $k = 4$ and (b) $k = 8$.

black dots are calculated based on Eqs. (46)–(49). For stable $G(s)$, the real part of all the dominant roots must be negative.

In Figs. 6(a), 6(b) and 7(a), the frequency band that ensures the stability of $G(s)$ emerges as the overlap between the bands of $g(s, \rho_1)$ and $g(s, \rho_N)$. Specifically, in Fig. 7(b), where the coupling strength $k = 8$ exceeds $1/(1+\rho_5)$, thus fulfilling Eq. (55), the frequency band is determined only by $S(\omega, \rho_1) = S_{\rm A}(\omega)$, resulting in an extended frequency band.

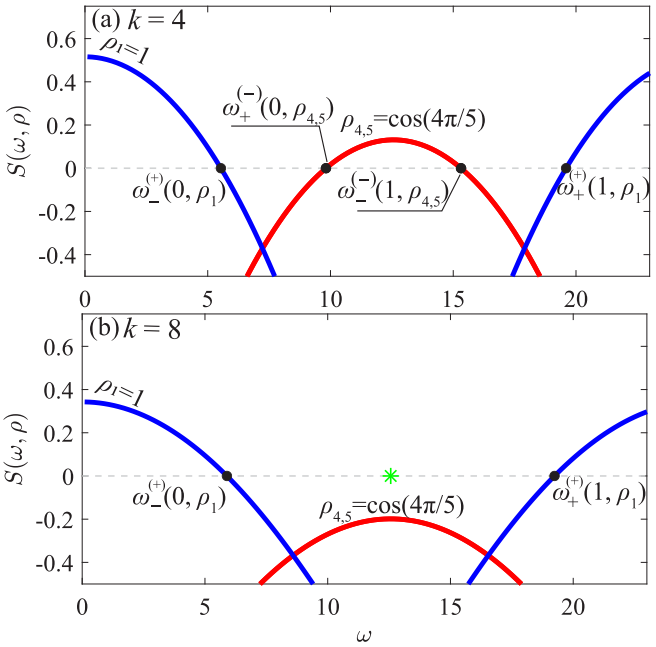

FIG. 7. Real part of dominant roots for $g(s, \rho_j) = 0$, $S(\omega, \rho)$, for ring network with $N = 5$ ($\tau = 0.25$): (a) $k = 4$ and (b) $k = 8$.

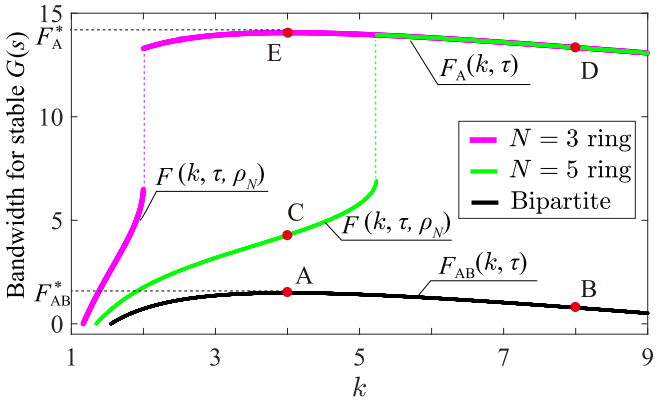

FIG. 8. Relationship between frequency bandwidth for stable $G(s)$ and coupling strength k ($\tau = 0.25$). Points A–D correspond to the parameters used in Figs. 6(a), 6(b), 7(a), and 7(b), respectively.

From Lemma 5, the frequency bandwidth can be classified into two types according to (k, τ) as follows.

Corollary 3. Under Eq. (53), the frequency bandwidth for stable $G(s)$ is given by

$$F(k,\tau,\rho_N) := \frac{\pi - \Phi(\rho_N,k) - \Phi(1,k)}{\tau} - \sqrt{D(\rho_N,k)} - \sqrt{D(1,k)}. \tag{56}$$

In addition, under Eq. (55), the frequency bandwidth for stable $G(s)$ is given by Eq. (26).

Proof. Under Eq. (53), the frequency bandwidth in Ω of Eq. (56) is calculated as $\omega_+^{(-)}(l,\rho_N) - \omega_-^{(+)}(l,1) = \omega_+^{(+)}(l,1) - \omega_-^{(-)}(l,\rho_N)$. ■

Notably, $F(k,\tau,\rho_N)$ and $F_{\rm A}(k,\tau)$ remain consistent for all l values. Furthermore, the condition for the frequency bandwidth $F(k,\tau,\rho_N)$ to be a minimum with respect to ρ_N is derived.

Corollary 4. For bipartite networks, the frequency bandwidth $F(k,\tau,\rho_N)$ takes a minimum value with respect to ρ_N and is given by Eq. (30).

Proof. By differentiating $F(k,\tau,\rho_N)$ with respect to ρ_N, we see that $F(k,\tau,\rho_N)$ shrinks with decreasing ρ_N and takes a minimum value when $\rho_N = -1$. It is known that the minimum eigenvalue is $\rho_N = -1$ if and only if the network is bipartite [65]. ■

Corollary 4 implies that bipartite networks exhibit limited robustness to frequency variations. Figure 8 illustrates the relationship between the frequency bandwidth for stable $G(s)$ and the coupling strength k for different network topologies: bipartite networks with $\rho_N = -1$, and ring networks with $N = 3$ ($\rho_3 = -0.5$) and $N = 5$ ($\rho_5 = \cos(4\pi/5) \simeq -0.8090$), with the connection delay consistently set at $\tau = 0.25$. The frequency bandwidth calculations employ $F_{\rm A}(k,\tau)$ from Eq. (26), $F(k,\tau,\rho_N)$ from Eq. (56), and $F_{\rm AB}(k,\tau)$ from Eq. (30), with points A–D representing the parameter sets used in Figs. 6(a), 6(b), 7(a), and 7(b), respectively.

For bipartite networks, such as networks with $N = 2$ or a ring network with $N = 12$, the bandwidth is notably narrower compared to nonbipartite networks, as depicted by the black curve against the pink and green curves for networks with $N = 3$ and $N = 5$. The bandwidth jumps at $k = 1/(1+\rho_N)$, namely, $k = 2$ for the ring network with $N = 3$ and $k \simeq 5.24$ for the ring network with $N = 5$ (see the pink and green dotted lines). This increase signifies that, beyond this threshold, the stability of $G(s)$ is governed only by $g_{\rm A}(s)$, particularly evident in Fig. 7(b).

The observations from Fig. 8 highlight a strategic approach to achieving extensive frequency bands: steering clear of bipartite networks and, in the case of ring networks with an odd number of oscillators, avoiding large values of N. This is because the minimum eigenvalue, ρ_N, tends towards -1 as N increases, diminishing the robustness against frequency variations [65].

B. Design procedure for oscillator networks

Based on the previous section, we propose a design procedure for oscillator networks that is robust against frequency variation. We consider the situation where the natural frequency $\omega = \omega_n$ and the minimum eigenvalue ρ_N are given. Similar to the case with $N = 2$, the design guideline is to set the coupling parameters such that the center of the frequency band is aligned with ω_n and that the frequency bandwidth is maximized.

Let us first consider the frequency band for stable $G(s)$ under Eq. (55), which is given by Eq. (22). The natural frequency ω_n aligns with the first center frequency $C_{\rm A}(1)$ in Eq. (24) when

$$\tau = \frac{\pi}{\omega_n} = 2\tau^*. \tag{57}$$

If $\tau^* < 1/2$, the frequency bandwidth $F_{\rm A}(k, 2\tau^*)$ is maximized with respect to k at $k = 1/(2\tau^*)$:

$$F_{\rm A}^* := F_{\rm A}(k^*/2, 2\tau^*) = \frac{2\omega_n}{\pi}\left(\pi - \phi\left(\frac{\omega_n}{\pi}\right)\right) - 2\sqrt{\frac{2\omega_n}{\pi} - 1}. \tag{58}$$

The sufficient condition for $F_{\rm A}(k, 2\tau^*)$ to be positive is given by

$$k \in \left(\frac{1}{1+\rho_N}, \frac{\omega_n^2}{8} + \frac{1}{2}\right). \tag{59}$$

We now derive a design procedure for nonbipartite networks with $\rho_N > -1$, where the following three specifications are satisfied: (i) the stability of $G(s)$ is governed only by $g_{\rm A}(s)$, (ii) the center of the frequency band for $g_{\rm A}(s)$ aligns with the natural frequency ω_n, and (iii) the frequency bandwidth $F_{\rm A}(k,\tau)$ is maximized with respect to k.

Theorem 2. Assume that ω_n and $\rho_N > -1$ satisfy

$$\omega_n > \frac{\pi}{1+\rho_N}. \tag{60}$$

For $(k,\tau) = (k^*/2,\ 2\tau^*)$, the local stability of steady state (39) is maintained even if the frequency changes by up to $\pm F_{\rm A}^*/2$.

Proof. Under Eq. (60), Eq. (55) is satisfied for $(k,\tau) = (k^*/2,\ 2\tau^*)$ and $\tau^* < 1/2$ holds. Therefore, for $(k,\tau) = (k^*/2,\ 2\tau^*)$, the stability of $G(s)$ is determined only by $g_{\rm A}(s)$ and the frequency bandwidth is given by Eq. (58). ■

Our design is categorized into three distinct scenarios based on the provided values of ω_n and ρ_N:

Case (i) $\rho_N = -1$ and ω_n satisfies Eq. (35):
From Corollary 4, the frequency band for $G(s)$ is the same as that for $g_{\mathrm{AB}}(s)$. Utilizing Theorem 1 to set the parameters ensures that the center of the frequency band for $g_{\mathrm{AB}}(s)$ aligns with ω_n, and the frequency bandwidth is maximized with respect to k. The designed parameter can maintain the stability amidst frequency changes up to $\pm F^*_{\mathrm{AB}}/2$, as demonstrated at point A in Fig. 8.

Case (ii) $\rho_N > -1$ and $\omega_n > \frac{\pi}{1+\rho_N}$:
By setting the parameters based on Theorem 2, the stability of $G(s)$ is governed only by $g_{\mathrm{A}}(s)$. These parameters ensure that the center of the frequency band of $g_{\mathrm{A}}(s)$ is aligned with ω_n and the frequency bandwidth is maximized. The designed parameters can maintain the stability for frequency shifts of up to $\pm F^*_{\mathrm{A}}/2$, highlighted at point E in Fig. 8.

Case (iii) $\rho_N > -1$ and $\omega_n \leqslant \frac{\pi}{1+\rho_N}$:
The stability of $G(s)$ is governed only by $g_{\mathrm{A}}(s)$ if the coupling strength satisfies Eq. (59). Additionally, setting the connection delay by Eq. (57) ensures that the center of the frequency band is aligned with ω_n. It is noteworthy, however, that this scenario does not entail maximized frequency bandwidth, with the tolerable frequency variation being $\pm F_A(k, 2\tau^*)/2$, as indicated at point D in Fig. 8.

It is important to highlight that in case (iii), while any k satisfying Eq. (59) is available, excessively high values of k are generally discouraged in practical engineering contexts, such as thermoacoustic systems [33], due to the monotonic decline of F_{A} with increases in k beyond $1/\tau$. The above design can be applied to various network topologies, ensuring resilience to frequency variations.

In the first example, a natural frequency $\omega_n = 2\pi$ and a minimum eigenvalue $\rho_N = -1$, which corresponds to bipartite networks such as ring networks with $N = 2$ and $N = 12$, are given. Since the minimum eigenvalue is $\rho_N = -1$ and $\omega_n = 2\pi$ satisfies Eq. (35), the design is performed according to case (i). According to Theorem 1, the coupling parameters are determined as $(k, \tau) = (4, 0.25)$. With these coupling parameters, ω_n is equal to the center of the frequency band, as depicted by the green star in Fig. 6(a). Moreover, the black curve in Fig. 8 demonstrates that the frequency bandwidth reaches its maximum at $k = 4$ (see point A). The allowable frequency variation, $\pm F^*_{\mathrm{AB}}/2$, is approximately ± 0.747 (or approximately $\pm 12\%$ of ω_n). Figure 9(a) shows the time-series data for $\mathrm{Re}[z_{1,\ldots,12}(t)]$ for a ring network with $N = 12$, using the designed parameters, under frequency variations. The frequency ω shifts from $\omega_n = 2\pi$ as follows: $\omega = 2\pi$ for $t \in [0, 40)$, $\omega = 2\pi + 0.6$ for $t \in [40, 80)$, and $\omega = 2\pi - 0.6$ for $t \in [80, 120]$. Notably, the oscillators remain quenched even with these frequency changes.[3]

In the second example, we examine a scenario with $\omega_n = 4\pi$ and $\rho_N = -0.5$, corresponding to a ring network with

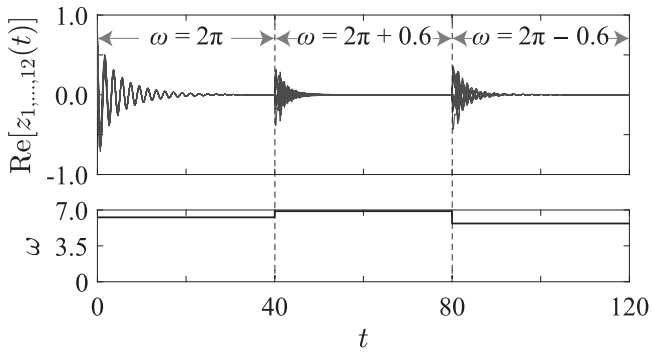

(a) Ring network with $N = 12$

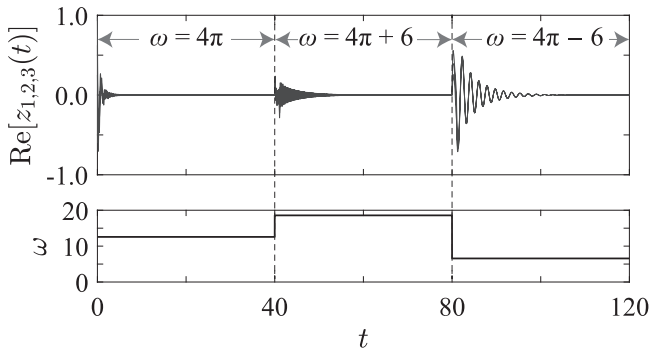

(b) Ring network with $N = 3$

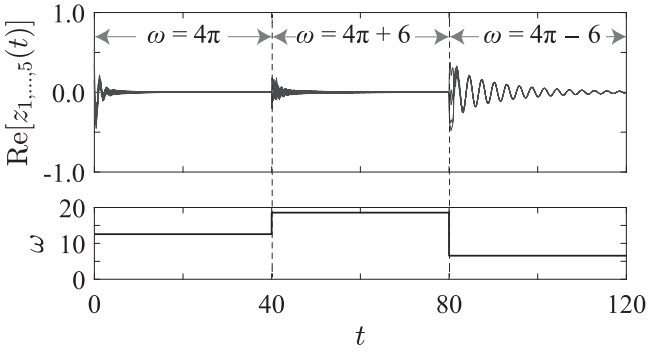

(c) Ring network with $N = 5$

FIG. 9. Time-series data for coupled oscillators with designed coupling parameters and that for frequency variation.

$N = 3$. These values satisfy $\omega_n > \frac{\pi}{1+\rho_N} = 2\pi$, leading to the application of case (ii) for parameter design. Consequently, the parameter set (k, τ) is chosen as $(k, \tau) = (4, 0.25)$. The pink curve in Fig. 8 confirms that the frequency bandwidth is maximized at $k = 4$ (see point E). The allowable frequency width, $\pm F^*_{\mathrm{A}}/2$, is approximately ± 7.03 (equivalent to approximately $\pm 56\%$ from ω_n). Figure 9(b) shows the time-series data for an $N = 3$ ring network with the designed parameter set. The frequency of the oscillators undergoes the following changes: $\omega = 4\pi$ for $t \in [0, 40)$, $\omega = 4\pi + 6$ for $t \in [40, 80)$, and $\omega = 4\pi - 6$ for $t \in [80, 120]$. Despite the considerable frequency variation, the oscillations are effectively suppressed.

In the third example, $\omega_n = 4\pi$ and $\rho_N = \cos(4\pi/5)$, corresponding to a ring network with $N = 5$, are given. Since the condition $\omega_n \leqslant \frac{\pi}{1+\rho_N} \simeq 5.24\pi$ is met, the design follows

[3]In our simulation, a uniform random external force within the range $[-5, 5]$ was applied to the right-hand side of Eq. (37) for all oscillators at $t = 40$ and 80.

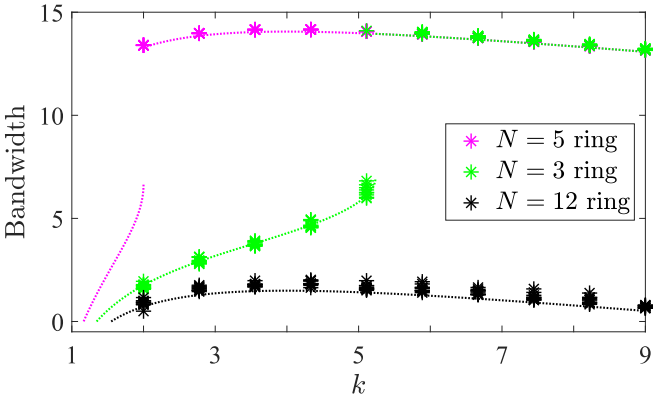

FIG. 10. Frequency bandwidth with frequency mismatch. The star marks show the numerical results with the frequency mismatch of variance 0.5, and the dotted curves are the analytical results without frequency mismatch shown in Fig. 8.

case (iii). We select a coupling strength $k = 8$, in accordance with Eq. (59), and set the connection delay τ to 0.25 by Eq. (57). Then, the center of the frequency band is aligned with $\omega_n = 4\pi$, as indicated by the green star in Fig. 7(b). Notably, point D in Fig. 8 suggests that the chosen parameters do not maximize the frequency bandwidth. However, Eq. (26) ensures stability over a frequency variation of $\pm F_{\mathrm{A}}(8, 0.25)/2 \simeq \pm 6.67$ (approximately $\pm 53\%$ from ω_n). Time-series data for a ring network with $N = 5$, shown in Fig. 9(c), demonstrate that amplitude death is sustained despite frequency variations, following the same frequency change pattern as in Fig. 9(b).

V. DISCUSSION

This section discusses the following: the effect of frequency mismatch on the frequency band for amplitude death, a comparison of parameter designs in this paper and previous studies, and a potential extension to coupled high-dimensional oscillators.

In the previous sections, for theoretical analysis, we assume an ideal situation where all the oscillators have the same frequency (i.e., no frequency mismatch). However, this is practically impossible. Therefore, we numerically investigate how the frequency mismatch affects the frequency bandwidth in which amplitude death occurs. Figure 10 shows the numerical results of the frequency bandwidth with frequency mismatch for $N = 3$, 5, and 12 ring networks. The connection delay is fixed at $\tau = 0.25$. Uniform random values with a variance of 0.5 are added to the oscillator frequencies in Eq. (37) to create frequency mismatch while fixing the mean frequency. The frequency bandwidth is estimated by calculating the dominant root in a linearized system containing the frequency mismatch around steady state (39) using an m-file function in MATLAB called eigAM [66]. Ten trials are performed for each coupling strength k. The star marks show the numerical results accounting for the frequency mismatch, and the dotted curves are the analytical results without frequency mismatch shown in Fig. 8. Even with the frequency mismatch, the bandwidth does not change significantly compared to the situation without mismatch. This result suggests that our no-frequency mismatch design procedure may be beneficial in situations with frequency mismatch. A detailed investigation of the relationship between frequency mismatch and the frequency bandwidth for amplitude death will be studied in the future.

Here, we introduce the parameter designs for inducing amplitude death in delay-coupled oscillators proposed in previous studies and compare them with the parameter design proposed in this paper. The design procedure for delay-coupled high-dimensional oscillator networks was proposed in Ref. [67]. The design does not depend on the topology of oscillator networks. Previous studies [68,69] proposed the design procedures for multiple delay connections and time-varying delay connections, respectively. These designs can induce amplitude death independently of delays. The design for Cartesian product networks of two subnetworks was proposed in Ref. [70]. This design does not require any information on the topologies of the subnetworks. In the above studies, parameters of oscillators (e.g., frequency) are assumed to be constant. Therefore, the robustness of these designs against frequency variations is yet to be investigated. Conversely, this paper focuses on robustness toward frequency variation. Furthermore, our analytical method may be applicable for other delay connections.

This paper considers coupled Stuart-Landau oscillators, in which each oscillator is described by a two-dimensional ordinary differential equation. In general, each oscillator in real applications would have higher dimension. Recently, a coupled generalized high-dimensional Stuart-Landau oscillator, which can capture rich dynamics in many real systems, has been proposed [71]. An extension of our paper's results to the high-dimensional oscillators should be considered in the future, enhancing their applicability across various applications.

VI. CONCLUSION

This paper investigated the frequency band for amplitude death in delay-coupled oscillators. The relationship between the oscillator frequency and the coupling parameters for inducing amplitude death was derived. We found that the frequency bandwidth is maximized when the coupling strength is inversely proportional to the connection delay. The paper also revealed that the frequency bandwidth is influenced by the minimum eigenvalue of the normalized adjacency matrix, and that bipartite networks exhibit limited resilience to frequency variations. Building on these insights, we proposed a robust design procedure applicable to a variety of network topologies that is robust against frequency variations. The efficacy of this design procedure was validated through a series of numerical simulations.

ACKNOWLEDGMENTS

This work was supported in part by JSPS KAKENHI (No. JP23K11245 and No. JP21H03513).

APPENDIX: PROOF OF LEMMA 5

Here, we show the following: (i) the frequency set for stable $G(s)$ is given by the intersection of Ω_{ρ_1} and Ω_{ρ_N}; (ii) Eq. (53) is the necessary and sufficient condition for the

existence of the intersection of Ω_{ρ_1} and Ω_{ρ_N}; and (iii) for $k > 1/(1+\rho_N)$, $G(s)$ is stable if and only if ω belongs to $\Omega_{\rm A}$.

For (i), $G(s)$ is stable if and only if $g(s,\rho)$ with an uncertain parameter is stable for any $\rho \in [\rho_N, 1]$. We apply the stability criterion of a quasipolynomial with uncertain parameters [60]:

$$p(s) = s - \alpha - \beta e^{-s\tau}. \tag{A1}$$

Let β be the uncertain parameter $\beta = \beta^r e^{i\beta^\theta}$, where $\beta^r \in [\underline{\beta}^r, \overline{\beta}^r]$ and $0 \leqslant \underline{\beta}^r \leqslant \overline{\beta}^r$. For fixed $\alpha \in \mathbb{C}$ and β^θ, the real part of the dominant root for the quasipolynomial (A1) is given by (see Lemma 6 in Ref. [60])

$$\begin{aligned}&\max\{S_w(\alpha,\beta) \mid \beta^r \in [\underline{\beta}^r, \overline{\beta}^r]\}\\ &\quad = \max\{S_w(\alpha, \underline{\beta}^r e^{i\beta^\theta}), S_w(\alpha, \overline{\beta}^r e^{i\beta^\theta})\},\end{aligned} \tag{A2}$$

where

$$S_w(\alpha,\beta) := \frac{1}{\tau}{\rm Re}[W_0(\tau\beta e^{-\alpha\tau})] + {\rm Re}[\alpha]. \tag{A3}$$

Equation (A2) implies that the quasipolynomial (A1) is stable for any $\beta^r \in [\underline{\beta}^r, \overline{\beta}^r]$ if and only if Eq. (A1) is stable for both $\underline{\beta}^r$ and $\overline{\beta}^r$. Let us apply the above to $g(s,\rho)$. Since ρ_N is always negative, we consider the following two cases: $\rho \in [\rho_N, 0]$ and $\rho \in [0, 1]$. For the former case, $g(s,\rho)$ is represented by Eq. (A1) with $\alpha = 1-k+i\omega$, $\underline{\beta}^r = 0$, $\overline{\beta}^r = -k\rho_N$, and $\beta^\theta = \pi$; thus, $g(s,\rho)$ is stable for any $\rho \in [\rho_N, 0]$ if and only if $g(s,\rho_N)$ and $g(s,0)$ are stable. For the latter case, $g(s,\rho)$ is represented by Eq. (A1) with $\alpha = 1-k+i\omega$, $\underline{\beta}^r = 0$, $\overline{\beta}^r = k$, and $\beta^\theta = 0$. $g(s,\rho)$ is stable for any $\rho \in [0, 1]$ if and only if $g(s,0)$ and $g(s,1)$ are stable. Therefore, $G(s)$ is stable if and only if $g(s,0)$, $g(s,1)$, and $g(s,\rho_N)$ are stable. $g(s,0)$ is stable independent of ω if $k > 1$. Hence, the frequency set for stable $G(s)$ is given by the intersection of that for $g(s,1)$ and that for $g(s,\rho_N)$ (i.e., $\Omega_{\rho_1} \cap \Omega_{\rho_N}$). We can see that Ω in Eq. (54) represents $\Omega_{\rho_1} \cap \Omega_{\rho_N}$.

For (ii), from Eqs. (44) and (45), the frequency band for $g(s,\rho)$ appears periodically with increasing ω. The center of the frequency band is given by Eq. (24) for $g(s,\rho_1)$ and Eq. (25) for $g(s,\rho_N)$. Thus, the intersection of Ω_{ρ_1} and Ω_{ρ_N} exists if and only if $\omega_+^{(-)}(l,\rho_N) - \omega_-^{(+)}(l,\rho_1) > 0$. This inequality can be rewritten as

$$\tau < \frac{\pi - \Phi(\rho_N,k) - \Phi(1,k)}{\sqrt{D(\rho_N,k)} + \sqrt{D(1,k)}}. \tag{A4}$$

Furthermore, to guarantee that the right-hand side of Eq. (A4) is positive, the coupling strength k must satisfy

$$k > 1. \tag{A5}$$

Additionally, the frequency sets Ω_{ρ_1} and Ω_{ρ_N} exist when Eq. (43) holds for $\rho = \rho_1$ and $\rho = \rho_N$. Thus, the intersection of Ω_{ρ_1} and Ω_{ρ_N} exists if and only if Eqs. (A4), (A5), and (43) with $\rho = \rho_1$ and $\rho = \rho_N$ are satisfied. These conditions are summarized as Eq. (53).

For (iii), assume that $\rho_N \neq -1$. From Corollary 2, $g(s,\rho)$ with any negative $\rho \in (0, \rho_N]$ is stable independent of ω for $k > \frac{1}{1-|\rho_N|} = \frac{1}{1+\rho_N}$. As shown in (i), $g(s,\rho)$ with $\rho \geqslant 0$ is stable if and only if $g(s,0)$ and $g(s,1) \equiv g_{\rm A}(s)$ are stable. $g(s,0)$ is stable independent of ω for $k > 1$. Under Eq. (20), $g(s,1)$ is stable if and only if ω belongs to $\Omega_{\rm A}$. Thus, under Eq. (55), $G(s)$ is stable if and only if ω is contained in $\Omega_{\rm A}$.

From (i)–(iii), the lemma is proven.

[1] A. Pikovsky, M. Rosenblum, and J. Kurths, *Synchronization* (Cambridge University Press, Cambridge, 2001).

[2] M. Chen, IEEE Trans. Circuits Syst. I Regul. Pap. **55**, 1335 (2008).

[3] Y. Xia and X. Liu, IEEE Trans. Circuits Syst. II **70**, 3514 (2023).

[4] P. DeLellis, M. di Bernardo, T. E. Gorochowski, and G. Russo, IEEE Circuits Syst. Mag. **10**, 64 (2010).

[5] K. A. Tsakalos, P. Dragkola, R. E. Karamani, M. A. Tsompanas, A. Provata, P. Dimitrakis, A. I. Adamatzky, and G. C. Sirakoulis, IEEE Trans. Circuits Syst. I **69**, 4128 (2022).

[6] L. Wetzel, D. Prousalis, R. F. Riaz, C. Hoyer, N. Joram, J. Fritzsche, F. Ellinger, and F. Jülicher, IEEE Access **10**, 80027 (2022).

[7] S. H. Chen, C. C. Chu, C. H. Hsia, and M. C. Shiue, IEEE Trans. Circuits Syst. I **69**, 757 (2022).

[8] S. K. Joshi, IEEE Trans. Circuits Syst. II **69**, 1737 (2022).

[9] Q. Song, G. Lu, G. Wen, J. Cao, and F. Liu, IEEE Trans. Circuits Syst. I **66**, 2723 (2019).

[10] G. Saxena, A. Prasad, and R. Ramaswamy, Phys. Rep. **521**, 205 (2012).

[11] W. Zou, D. V. Senthilkumar, M. Zhan, and J. Kurths, Phys. Rep. **931**, 1 (2021).

[12] Y. Sugitani and K. Konishi, NOLTA, IEICE **12**, 612 (2021).

[13] N. Zhao and X. Zhang, Physica A **622**, 128803 (2023).

[14] N. Zhao, Z. Sun, X. Song, and Y. Xiao, Physica A **608**, 128288 (2022).

[15] A. Ghosh, S. Mondal, and R. I. Sujith, Chaos **32**, 101106 (2022).

[16] N. Zhao, Z. Sun, X. Song, and Y. Xiao, Physica D **439**, 133434 (2022).

[17] D. G. Aronson, G. B. Ermentrout, and N. Kopell, Physica D **41**, 403 (1990).

[18] K. Konishi and N. Hara, Phys. Rev. E **83**, 036204 (2011).

[19] A. Prasad, M. Dhamala, B. M. Adhikari, and R. Ramaswamy, Phys. Rev. E **81**, 027201 (2010).

[20] W. Zou, S. He, and C. Yao, Appl. Math. Lett. **131**, 108052 (2022).

[21] S. H. Strogatz, Nature (London) **394**, 316 (1998).

[22] D. V. R. Reddy, A. Sen, and G. L. Johnston, Phys. Rev. Lett. **80**, 5109 (1998).

[23] D. V. R. Reddy, A. Sen, and G. L. Johnston, Phys. Rev. Lett. **85**, 3381 (2000).

[24] Y. Sugitani, K. Konishi, and N. Hara, Nonlinear Dyn. **70**, 2227 (2012).

[25] S. Masamura, T. Iwamoto, Y. Sugitani, K. Konishi, and N. Hara, Nonlinear Dyn. **99**, 3155 (2020).

[26] S. Ansari, J. Zhang, and R. E. Singh, Prot. Control Mod. Power Syst. **7**, 2 (2022).

[27] R. Kumar and C. N. Bhende, Energies **16**, 1339 (2023).
[28] S. K. Subudhi and S. Maity, in *2018 International Conference on Power, Instrumentation, Control and Computing (PICC)* (IEEE, 2018), pp. 1–5.
[29] S. R. Huddy and J. D. Skufca, IEEE Trans. Power Electron. **28**, 247 (2013).
[30] T. Poinsot, Proc. Combust. Inst. **36**, 1 (2017).
[31] R. I. Sujith and S. A. Pawar, *Thermoacoustic Instability* (Springer, Switzerland, 2021).
[32] R. I. Sujith and V. R. Unni, Phys. Fluids **32**, 061401 (2020).
[33] T. Biwa, S. Tozuka, and T. Yazaki, Phys. Rev. Appl. **3**, 034006 (2015).
[34] H. Hyodo and T. Biwa, Phys. Rev. E **98**, 052223 (2018).
[35] A. Sahay, A. Roy, S. A. Pawar, and R. I. Sujith, Phys. Rev. Appl. **15**, 044011 (2021).
[36] N. Thomas, S. Mondal, S. A. Pawar, and R. I. Sujith, Chaos **28**, 093116 (2018).
[37] N. Thomas, S. Mondal, S. A. Pawar, and R. I. Sujith, Chaos **28**, 033119 (2018).
[38] S. Srikanth, S. A. Pawar, K. Manoj, and R. I. Sujith, Chaos **32**, 073129 (2022).
[39] M. H. Doranehgard, V. Gupta, and L. K. B. Li, Phys. Rev. E **105**, 064206 (2022).
[40] H. Hyodo, M. Iwasaki, and T. Biwa, J. Appl. Phys. **128**, 094902 (2020).
[41] S. Dange, K. Manoj, S. Banerjee, S. A. Pawar, S. Mondal, and R. I. Sujith, Chaos **29**, 093135 (2019).
[42] H. Jegal, K. Moon, J. Gu, L. K. B. Li, and K. T. Kim, Combust. Flame **206**, 424 (2019).
[43] K. Moon, Y. Guan, L. K. B. Li, and K. T. Kim, Chaos **30**, 023110 (2020).
[44] Y. Guan, K. Moon, K. T. Kim, and L. K. B. Li, Phys. Rev. E **104**, 024216 (2021).
[45] R. Delage, Y. Takayama, and T. Biwa, Chaos **27**, 043111 (2017).
[46] R. Delage, Y. Takayama, and T. Biwa, Chaos **28**, 083125 (2018).
[47] M. Cai, J. K. Liu, and J. Li, Appl. Math. Mech. **27**, 953 (2006).
[48] A. Raj, A. Raaj, J. Venkatramani, and S. Mondal, Chaos **31**, 123112 (2021).
[49] A. Raaj, S. Mondal, and J. Venkatramani, Int. J. Non Linear Mech. **129**, 103659 (2021).
[50] W. Du, K. Zheng, and H. Wang, IET Gener. Transm. Distrib. **13**, 2637 (2019).
[51] L. Guo, S. Zhang, X. Li, Y. W. Li, C. Wang, and Y. Feng, IEEE J. Emerg. Sel. Topics Power Electron. **5**, 338 (2017).
[52] K. Rajagopal, Y. Admassu, R. Weldegiorgis, P. Duraisamy, and A. Karthikeyan, Complexity **2019**, 1 (2019).
[53] E. Hossain, R. Perez, A. Nasiri, and S. Padmanaban, IEEE Access **6**, 33285 (2018).
[54] Z. Li, J. B. Park, Y. H. Joo, B. Zhang, and G. Chen, IEEE Trans. Circuits Syst. I **49**, 383 (2002).
[55] D. Premraj, K. Manoj, S. A. Pawar, and R. I. Sujith, Nonlinear Dyn. **103**, 1439 (2021).
[56] J. Guckenheimer and P. Holmes, *Nonlinear Oscillations, Dynamical Systems, and Bifurcations of Vector Fields* (Springer, New York, 1983).
[57] P. Hövel, *Control of Complex Nonlinear Systems with Delay* (Springer, Berlin, 2010).
[58] A. Balanov, N. Janson, and O. Sosnovtseva, *Synchronization: From Simple to Complex* (Springer, Berlin, 2008).
[59] L. Illing, Phys. Rev. E **94**, 022215 (2016).
[60] H. Shinozaki and T. Mori, Automatica **42**, 1791 (2006).
[61] R. M. Corless, G. H. Gonnet, D. E. G. Hare, D. J. Jeffrey, and D. E. Knuth, Adv. Comput. Math. **5**, 329 (1996).
[62] C. U. Choe, R. S. Kim, P. Hövel, and E. Schöll, Int. J. Dyn. Control **4**, 123 (2016).
[63] P. van Mieghem, *Graph Spectra for Complex Networks* (Cambridge University Press, Cambridge, 2010).
[64] E. Fridman, *Introduction to Time-Delay Systems* (Birkhäuser Cham, Switzerland, 2014).
[65] F. Chung, *Spectral Graph Theory* (American Mathematical Society, Rhode Island, 1997).
[66] D. Breda, S. Maset, and R. Vermiglio, *Stability of Linear Delay Differential Equations: A Numerical Approach with MATLAB* (Springer, New York, 2015).
[67] Y. Sugitani, K. Konishi, L. B. Le, and N. Hara, Chaos **24**, 043105 (2014).
[68] K. Konishi, H. Kokame, and N. Hara, Phys. Rev. E **81**, 016201 (2010).
[69] Y. Sugitani, K. Konishi, and N. Hara, Phys. Rev. E **92**, 042928 (2015).
[70] Y. Sugitani and K. Konishi, Phys. Rev. E **96**, 042216 (2017).
[71] W. Zou, S. He, D. V. Senthilkumar, and J. Kurths, Phys. Rev. Lett. **130**, 107202 (2023).